A Combined Spectroscopic, Photophysical and Theoretical (DFT) Study of the Electronically Excited Inorganometallic Complexes [Ru(E)(E')(CO)$_2$(*i*Pr–DAB)] (E = Cl, Me, SnPh$_3$, PbPh$_3$; E' = GePh$_3$, SnR$_3$, PbR$_3$ (R = Me, Ph); *i*Pr–DAB = *N*,*N*'-diisopropyl-1,4-diaza-1,3-butadiene): Evidence of an Exceptionally Long-Lived $^3\sigma\pi^*$ Excited State for [Ru(SnPh$_3$)$_2$(CO)$_2$(*i*Pr–DAB)]

Maxim P. Aarnts, Derk J. Stufkens,* Maikel P. Wilms, Evert Jan Baerends, Antonín Vlček, Jr.,* Ian P. Clark, Michael W. George and James J. Turner

Abstract: The photophysical properties of the metal–metal bonded complexes [Ru(E)(E')(CO)$_2$(*i*Pr–DAB)] (E = Cl, E' = SnPh$_3$, PbPh$_3$; E = Me, E' = SnPh$_3$, PbPh$_3$; E = SnPh$_3$, E' = SnMe$_3$, SnPh$_3$, GePh$_3$; E = PbPh$_3$, E' = PbMe$_3$, PbPh$_3$, GePh$_3$; *i*Pr–DAB = *N*,*N*'-diisopropyl-1,4-diaza-1,3-butadiene) have been studied. According to time-resolved emission, UV/vis and IR spectra, combined with density functional (DFT) MO calculations, the lowest excited state has triplet metal-to-ligand charge-transfer (^{3}MLCT), triplet halide-to-ligand charge-transfer (^{3}XLCT) or $^3\sigma_{(E-Ru-E')}\pi^*$ character, depending on the nature and combination of the ligands E and E'. The $^3\sigma_{(E-Ru-E')}\pi^*$ state is a bound state whose lifetime is strongly influenced by the ligands E and E'. An exceptionally long lifetime (264 μs at 80 K) is observed for the $^3\sigma_{(Sn-Ru-Sn)}\pi^*$ state of the symmetrically substituted [Ru(SnPh$_3$)$_2$(CO)$_2$(*i*Pr–DAB)] complex. The reason for this long lifetime is the fact that the excited state of this complex is hardly distorted with respect to the ground state, owing to the delocalised character of the σ(Sn–Ru–Sn) bonding orbital, which mixes strongly with the π* orbital of the *i*Pr–DAB ligand. This delocalisation is also responsible for the unusually high oscillator strength of the σ → π* electronic transition in the visible spectral region.

Keywords
density functional calculations · IR spectroscopy · ruthenium complexes · time-resolved spectroscopy · UV/vis spectroscopy

Introduction

Recently, a new type of complex [Ru(E)(E')(CO)$_2$(α-diimine)] (E = halide, E' = alkyl; E = Me, E' = Mn(CO)$_5$; α-diimine = e.g. bpy, *i*Pr–DAB)[1–6] was synthesised and investigated in our laboratories. Initial studies on their spectroscopy, photophysics and photochemistry have clearly indicated their great potential as luminophores, photosensitisers and initiators of radical reactions, as well as the challenge they pose for the understanding of characters and dynamics of the excited states of organometallic compounds. In a way, the [Ru(E)(E')(CO)$_2$(α-diimine)] complexes resemble the better known [Re(X)(CO)$_3$(α-diimine)] species, whose various kinds of photoactivity and whose function as efficient photosensitisers have been amply demonstrated.[7–17] For the Re complexes, the nature of the lowest excited state may be tuned broadly from metal-to-ligand charge transfer (MLCT) to halide-to-ligand charge transfer (XLCT) to σπ* by changing the axial ligand X from Cl to I to alkyl or metal-containing fragment.[18–28] Each of these excited states was shown to have its own properties and dynamics. Further tuning of the excited state behaviour is possible by changing the α-diimine ligand.[28]

The excited-state properties of the [Ru(E)(E')(CO)$_2$(α-diimine)] complexes may be varied on a much broader scale than in the case of their Re analogues since the E and E' ligands at either of the two axial positions, as well as the α-diimine ligand, may be replaced independently. Thus, it has already been shown that the MLCT excited state of [Ru(Cl)(Me)(CO)$_2$(α-diimine)] changes into a longer-lived, emissive, XLCT state for [Ru(I)(Me)(CO)$_2$(α-diimine)],[5] while homolysis of the Ru–alkyl or Ru–Mn bond was found to occur from the $^3\sigma\pi^*$ excited state

[*] Derk J. Stufkens, Maxim P. Aarnts, Maikel P. Wilms
Anorganisch Chemisch Laboratorium, J. H. van't Hoff Research Institute
Universiteit van Amsterdam, Nieuwe Achtergracht 166, 1018 WV Amsterdam (The Netherlands)
Fax: Int. code +(20)525-6456
e-mail: stufkens@anorg.chem.uva.nl
Evert Jan Baerends
Afdeling Theoretische Chemie, Vrije Universiteit
De Boelelaan 1083, 1081 HV Amsterdam (The Netherlands)
Antonín Vlček Jr.
J. Heyrovský Institute of Physical Chemistry
Academy of Sciences of the Czech Republic
Dolejškova 3, 182 23 Prague (Czech Republic)
Present address: Dept. of Chemistry, Queen Mary and Westfield College
University of London, London E1 4NS (UK)
Ian P. Clark, Michael W. George, James J. Turner
Dept. of Chemistry, University of Nottingham, Nottingham NG7 2RD (UK)

0947-6539/96/0212-1556 $ 15.00+.25/0

of [Ru(I)(*i*Pr)(CO)$_2$(α-diimine)] and [Ru(Me)(Mn(CO)$_5$)(CO)$_2$-(α-diimine)], respectively.[4]

A whole range of new excited-state phenomena may be expected for the newly synthesised inorganometallic complexes [*trans,cis*-Ru(E)(E′)(CO)$_2$(*i*Pr–DAB)] in which E = Cl, E′ = $SnPh_3$, $PbPh_3$; E = Me, E′ = $SnPh_3$, $PbPh_3$; E = $SnPh_3$, E′ = $SnPh_3$, $SnMe_3$, $GePh_3$; E = $PbPh_3$, E′ = $PbPh_3$, $PbMe_3$, $GePh_3$, whose general structure is shown in Figure 1. Their spectroscopic[29] and electrochemical[30, 31] behaviour has already indicated that the bonding properties and electronic structures are quite different from those of analogous Re and Ru species discussed above. Importantly, depending on the nature of E and E′, there is a large variation in the electron distribution within the Ru(DAB) chelate ring. For complexes in which one axial ligand E is a halide or Otf^- ($SO_3CF_3^-$), the π-electron donation from the Ru(E)(E′) fragment to the DAB ligand remains very limited, leaving the bonding within the Ru(DAB) chelate ring rather localised. On the other hand, in the complexes where both E and E′ are coordinated through a Group 14 metal atom (Sn, Ge, Pb), as well as for [Ru(Me)(E′)(CO)$_2$(*i*Pr–DAB)] (E′ = $SnPh_3$, $PbPh_3$), rather strong interaction between the occupied orbitals of the Ru(E)(E′) unit and the π* DAB orbital occurs, resulting in extensive electron delocalisation. Compared with the former class of complexes, the latter more delocalised species are characterised by red-shifted visible absorption bands, much lower wavenumbers of the ν(CO) and ν_s(CN) vibrations, and by the appearance of resonantly enhanced Raman peaks attributed to ν(CC) and deformation vibrations of the DAB ligand and to skeletal vibrations. In addition, these complexes show several specific NMR features, for example, upfield-shifted resonances of the imine protons, and most strikingly, very large $^4J(^{117/119}Sn,H_{(imine)})$ coupling constants, as was described in ref. [29]. This electron delocalisation in the Ru(E)(E′)(DAB) unit is also manifested structurally by shorter C(1)–C(2) and longer C=N bond lengths in the DAB ligand of the [Ru($SnPh_3$)$_2$(CO)$_2$(*i*Pr–DAB)] complex relative to those of [Ru(Cl)($SnPh_3$)(CO)$_2$(*i*Pr–DAB)].[29] A detailed density-functional (DFT) MO theoretical study of [Ru(SnH_3)$_2$(CO)$_2$(H–DAB)] and spectroelectrochemical investigation of [Ru($SnPh_3$)$_2$(CO)$_2$(*i*Pr–DAB)][31] have shown that this delocalisation originates predominantly in a strong mixing between the occupied weakly bonding σ(Sn–Ru–Sn) orbital and the π* DAB orbital. This rather unusual σ–π* electron delocalisation in the [Ru(E)(E′)(CO)$_2$(*i*Pr–DAB)] complexes is also expected to influence profoundly the characters and dynamics of their excited states, which thus became the principle subjects of this study.

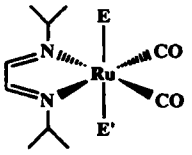

Fig. 1. Generalised structure of the [Ru(E)(E′)(CO)$_2$-(*i*Pr–DAB)] complexes.

Results and Discussion

As explained in the Introduction, the [Ru(E)(E′)(CO)$_2$(*i*Pr–DAB)] complexes may be divided into two classes with distinct spectroscopic (UV/vis, IR, rR, NMR) properties[29] that reflect different extents of electron delocalisation between the Ru(E)(E′) unit and the DAB ligand. The first class, hereinafter referred to as "halide", consists of complexes containing an electronegative ligand E = Cl, I or Otf in combination with E′ = Me, $SnPh_3$ or $PbPh_3$. The other class, hereinafter to be called "non-halide", consists of complexes in which both E and E′ are inorganometallic ligands ($GePh_3$, $SnPh_3$, $SnMe_3$, $PbPh_3$ or $PbMe_3$), and of species where E = Me and E′ = $SnPh_3$ or $PbPh_3$. In the following sections, the UV/vis and rR spectra of both these classes of [Ru(E)(E′)(CO)$_2$(*i*Pr–DAB)] complexes are used to provide information on their excited-state characters. This is followed by a discussion of the results of the steady-state emission measurements and the time-resolved emission, UV/vis and IR absorption studies.

Electronic absorption spectra: The halide complexes [Ru(Cl)-(E′)(CO)$_2$(*i*Pr–DAB)] (E′ = alkyl, $SnPh_3$, $PbPh_3$), are yellow-orange because of the presence of a strong absorption band between 400–450 nm. The lowest energy absorption bands in the UV/vis spectra of the red-purple compounds of the non-halide class are observed at longer wavelengths, between 510 and 575 nm in THF, with extinction coefficients approximately twice as large as those of the halide species. The [Ru($PbPh_3$)$_2$(CO)$_2$(*i*Pr–DAB)] complex has a shoulder on the high-energy side of its absorption band which becomes even more pronounced at 77 K.[29] The lowest energy absorption band of [Ru($SnPh_3$)$_2$(CO)$_2$(*i*Pr–DAB)] has no shoulder at room temperature but at 77 K in a 2-MeTHF glass the band becomes somewhat asymmetric. The UV/vis spectroscopic data are summarised in Table 1 and representative spectra are shown in Figures 6 and 9.

Table 1. CO and CN stretching frequencies and visible spectral data for [Ru(E)-(E′)(CO)$_2$(*i*Pr–DAB)].

Complex E	Complex E′	IR [a] ν_s(CO)	IR [a] ν_{as}(CO)	rR [b] ν_s(CN) [c]	Visible absorption λ_{max} (ε) [d]	Visible absorption Δ [e]
Otf	$SnPh_3$	2040	1981			
Cl	Me [f]	2024	1952	1565 (2) [g]	435 (1710)	1870 [h]
I	Me [f]	2024	1958	1556 (2) [g]	463 (2320)	2320
Cl	$PbPh_3$	2028	1972	1541 (2)	444 (2520)	1560
Cl	$SnPh_3$	2027	1969	1543 (2)	435 (2850)	1710
$PbPh_3$	$GePh_3$	2007	1955	1476 (3)	538 (5920)	820
$SnPh_3$	$GePh_3$	2007	1953	1476 (3)	519 (5130)	740
Me	$PbPh_3$	2006	1949	[i]	537 (4600)	1450
$PbPh_3$	$PbPh_3$	2006	1956	1473 (3)	543 (4840)	940
$SnPh_3$	$SnPh_3$	2005	1952	1473 (3)	515 (6050)	710
Me	$SnPh_3$	2003	1946	1485 (3)	518 (5720)	1180
$PbPh_3$	$PbMe_3$	1999	1948	1471 (3)	550 (5460)	650
$SnPh_3$	$SnMe_3$	1994	1940	1471 (3)	514 (6230)	490

[a] IR (cm^{-1}) data were obtained in THF. [b] Resonance Raman data (cm^{-1}) were determined for the complex in a KNO_3 pellet. [c] The number in parentheses refers to the type of spectrum (Fig. 2 or 3). [d] Maxima (nm) of the visible absorption bands and their extinction coefficients ($M^{-1}cm^{-1}$) in parentheses were obtained in THF. [e] $\Delta = \tilde{\nu}_{max}(CH_3CN) - \tilde{\nu}_{max}$(hexane) in cm^{-1}. [f] From refs. [1, 62]. [g] Synthesised according to ref. [1]. [h] $\Delta = \tilde{\nu}_{max}(CH_3CN) - \tilde{\nu}_{max}$(toluene) in cm^{-1}. [i] No rR spectrum was obtained owing to high photolability.

The visible absorption band of the halide complexes shows a large solvatochromism, which is characteristic of CT transitions. Replacement of the chloride by the more electron-releasing ligands Me, $SnPh_3$ or $PbPh_3$ shifts the absorption band to lower energy with a concomitant decrease of solvatochromism. The latter effect, which points to a decrease in CT character, is due to increased mixing between the orbitals of the Ru(E)(E′)(CO)$_2$ fragment and the π* LUMO of the *i*Pr–DAB ligand (vide infra). This increased mixing is also reflected in a drop in the frequencies of the ν_s(CN) and ν(CO) vibrations (Table 1). Replacement of Me in [Ru(Cl)(Me)(CO)$_2$(*i*Pr–DAB)], [Ru(Me)($SnPh_3$)(CO)$_2$(*i*Pr–DAB)] or [Ru(Me)($PbPh_3$)(CO)$_2$-(*i*Pr–DAB)] by $SnPh_3$ or $PbPh_3$ always leads to a significant decrease of solvatochromism (Table 1), although the charge density at the central metal atom, as reflected in the ν(CO) frequencies,[29] hardly changes. This effect may be due to the steric shielding of the metal from the solvent by the bulky EPh_3

  0947-6539/96/0212-1557 $ 15.00+.25/0

groups. On the other hand, ν_s(CN) is still lowered in frequency (from 1485 to 1473 cm^{-1}) on replacement of Me in [Ru(Me)-($SnPh_3$)(CO)$_2$(*i*Pr-DAB)] by $SnPh_3$. Thus, π back-donation to the DAB ligand and solvatochromism depend much more on the nature of the axial ligands than π back-donation to the carbonyls does.

Resonance Raman spectra: In order to gain more insight into the character of the lowest electronic transitions of the complexes under investigation, we performed a resonance Raman (rR) study, using the fact that only those vibrations that are vibronically coupled to the resonant electronic transitions are normally enhanced. The wavelength of excitation was varied from 457.9 to 514.5 nm. In some cases, strong emission restricted the measurements to excitation at the high-energy side of the absorption band and to a relatively narrow wavenumber region, 100-1800 cm^{-1}. Figures 2 and 3 show rR spectra of [Ru(Cl)($SnPh_3$)-(CO)$_2$(*i*Pr-DAB)] and [Ru($SnPh_3$)$_2$(CO)$_2$(*i*Pr-DAB)], which

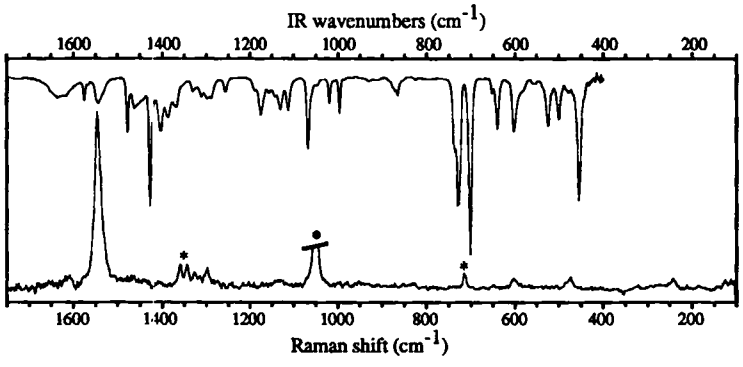

Fig. 2. IR (KBr, top) and rR (KNO_3, λ_{exc} = 476.5 nm, bottom) spectra of [Ru(Cl)($SnPh_3$)-(CO)$_2$(*i*Pr-DAB)].

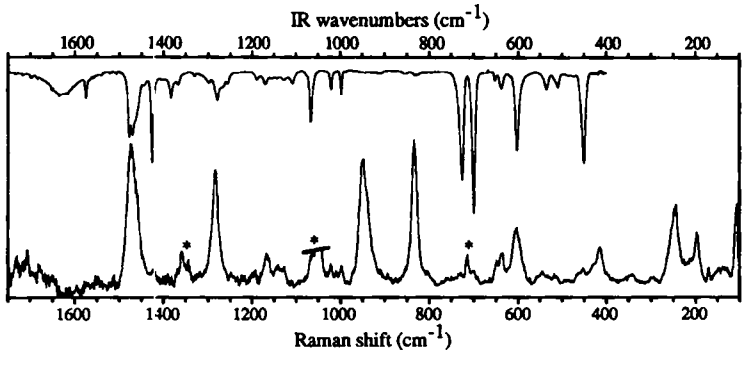

Fig. 3. IR (KBr, top) and rR (KNO_3, λ_{exc} = 472.8 nm, bottom) spectra of [Ru($SnPh_3$)$_2$(CO)$_2$-(*i*Pr-DAB)].

typify the rR spectral patterns of the complexes belonging to the halide and non-halide classes of compounds, respectively. Thus, the rR spectrum of [Ru(Cl)($SnPh_3$)(CO)$_2$(*i*Pr-DAB)] is very similar to those obtained for E = Cl, E' = Me, $PbPh_3$; E = I, E' = Me, Et[1] and E = Otf, E' = Me,[11] whereas the rR spectrum of [Ru($SnPh_3$)$_2$(CO)$_2$(*i*Pr-DAB)] closely resembles those of the complexes with E = $SnPh_3$, E' = Me, $GePh_3$ and E = $PbPh_3$, E' = $GePh_3$, $PbPh_3$. A complete list of the rR peaks is given in ref. [29].

All complexes studied show resonance enhancement of Raman intensity for the band attributed to the ν_s(CN) vibration of the *i*Pr-DAB ligand[32,33] (see Table 1 for the wavenumber values). This confirms that the electronic transitions in the visible spectral region are in all cases directed to the lowest π^* orbital of *i*Pr-DAB, whose occupation will primarily affect the C=N bonds, since it is antibonding with respect to these bonds. For the halide complexes, ν_s(CN) is, in fact, the only vibration showing a rR effect. The absence of a Raman band for ν_s(CO) is quite typical for an electronic transition having a predominant halide $\rightarrow \pi^*$ diimine (XLCT) character.[1,28] This XLCT character is confirmed by the DFT MO data to be discussed hereinafter.

Going from the halide complexes to those of the non-halide class, the wavenumber of the ν_s(CN) Raman peak drops by more than 70 cm^{-1} (Table 1), owing to increased π back-donation to *i*Pr-DAB. At the same time, the intensity pattern of the rR spectrum changes dramatically since the ν(CC) Raman peak at $\approx$1250 cm^{-1} and a group of Raman bands at wavenumbers below 1000 cm^{-1} become resonance-enhanced.

By analogy with the rR spectra of the [M{M(CO)$_5$}(CO)$_3$-(*i*Pr-DAB)] (M = Mn and/or Re) complexes studied earlier,[32] the peaks of [Ru($SnPh_3$)$_2$(CO)$_2$(*i*Pr-DAB)] at 950 and 833 cm^{-1} are attributed to deformations of the DAB ligand, while the bands at smaller wavenumbers (603, 418, 245, 196 cm^{-1}) belong to the metal-ligand stretching (e.g., ν(M-C), ν(M-N), ν(M-M)) and deformation (e.g., δ(M-C-O)) modes.[32,34] The enhancement of all these peaks points to a largely delocalised character of the resonant electronic transition. Obviously, several bonds and their angles within the Ru(DAB) chelate ring are influenced by electronic excitation. However, it should be noted that the overall rR effect, as estimated from the intensity ratio of the ν_s(CN) band and the $\nu_s(NO_3^-)$ reference band, is weaker for [Ru($SnPh_3$)$_2$(CO)$_2$(*i*Pr-DAB)] and its non-halide congeners than for the halide complexes. Apparently, CT excitation of the halide complexes strongly distorts only the C=N bonds, whereas in the case of the non-halide complexes the overall excited state distortion is smaller and distributed over many normal coordinates.

The non-halide complexes show a small splitting, sometimes manifested only as a broadening, of the ν_s(CN) band (see Fig. 3). This was also observed for other complexes (e.g., [Re{Mn(CO)$_5$}(CO)$_3$(*i*Pr-DAB)],[32] [Ru{M(CO)$_5$}$_2$(CO)$_2$(*i*Pr-DAB)] (M = Mn, Re)[35,36]). In some cases, for example [Ru($SnPh_3$){Mn(CO)$_5$}(CO)$_2$(*i*Pr-DAB)],[35] the IR band of the ν_s(CN) vibration, measured in KBr, also shows a small splitting. Probably there are two closely related conformers, for instance rotamers, having slightly different ν_s(CN) wavenumbers. The equilibrium between them must be very fast in fluid solution since they could not be observed with NMR, even at low temperature. The presence of these conformers may also explain the observation of two transient species in the low-temperature emission and TRIR spectra of [Ru($SnPh_3$)$_2$(CO)$_2$-(*i*Pr DAB)] (vide infra).

DFT MO calculations: To aid the interpretation of the spectroscopic results, DFT MO calculations were performed on [Ru(Cl)-(SnH_3)(CO)$_2$(H-DAB)] and [Ru(Me)(SnH_3)(CO)$_2$(H-DAB)] as model compounds for the halide and non-halide complexes, respectively. The electronic structure of the latter complex will also be discussed in relation to the results of the DFT MO calculation on [Ru(SnH_3)$_2$(CO)$_2$(H-DAB)] published previously.[31] It has to be realised, however, that the results of these DFT MO calculations should be used with care for explaining the excited state properties, since only the electronic wavefunction of the excited molecule at the ground-state geometry was calculated.

0947-6539/96/0212-1558 $ 15.00+.25/0 Chem. Eur. J. 1996, 2, No. 12

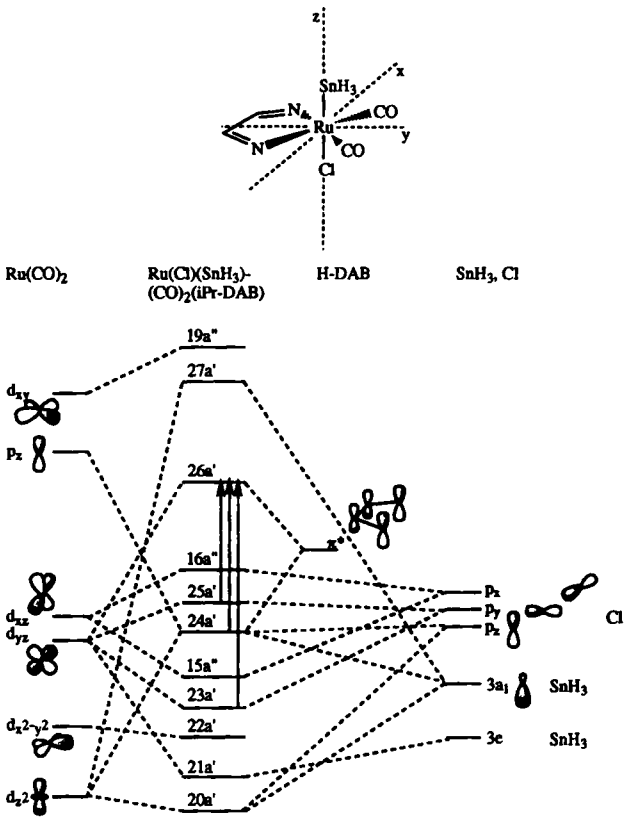

Fig. 4. Qualitative MO scheme of [Ru(Cl)(SnH$_3$)(CO)$_2$(H–DAB)] based on the DFT MO calculations; see also Table 2.

Figure 4 and Tables 2a and b show the results of the DFT MO calculation for [Ru(Cl)(SnH$_3$)(CO)$_2$(H–DAB)]. The occupied orbitals 16a", 25a', 15a" and 23a' can be described as π-interacting Ru d(π) and Cl p(π) orbitals. The 24a' HOMO-2 orbital has predominantly σ character with respect to the axial bonds. It is composed of the halide 3p$_z$ orbital (25%) and the sp^3 hybrid of SnH$_3$ 3a$_1$ (30%), together with the 5p$_z$ (10%) and 4d$_{z^2}$ (7%) orbitals of Ru. Both the 25a' HOMO-1 and 16a" HOMO have a strongly mixed Cl p(π)/Ru d(π) character, the Cl contribution dominating (79% and 67%, respectively). Unlike the 25a', the 16a" HOMO has a different symmetry from the π* DAB orbital, which has important spectroscopic consequences. The LUMO (26a') is composed mainly of this 2b$_1$ π* DAB orbital (69%), with only small contributions from other orbitals. This reflects the predominant chloride/ruthenium character of the HOMO-1 and HOMO on one side and the DAB-localised character of the LUMO on the other. The calculated orbital characters of [Ru(Cl)(SnH$_3$)(CO)$_2$(H–DAB)] closely resemble those of [Ru(Cl)(Me)(CO)$_2$(H–DAB)],[37] for which an MLCT type of excitation was found experimentally.[5] However, based on the DFT MO calculations, the halide contribution to the 16a" and 25a' orbitals is somewhat larger for [Ru(Cl)(SnH$_3$)(CO)$_2$(H–DAB)], and the transitions from these orbitals to the LUMO may better be described as having mixed MLCT/XLCT character.

On going to [Ru(Me)(SnH$_3$)(CO)$_2$(H–DAB)], the orbital diagram changes quite considerably, as can be seen from Table 3 and Figure 5. The HOMO is now of a σ character with respect

Table 2a. DFT-calculated characters and energies of the relevant MO's of [Ru(Cl)-(SnH$_3$)(CO)$_2$(H–DAB)] [a].

Orbital	Description	ε (eV)	Ru	SnH$_3$	Cl	H–DAB	CO
27a'	σ*	−2.401	29% d$_{z^2}$	21% 3a$_1$	12% p$_z$		19% 2π
26a'	**DAB π***	**−4.806**	**9% d$_{yz}$**	**5% 3a$_1$**	**10% p$_z$**	**69% 2b$_1$**	
16a"	**Ru–Cl π**	**−5.976**	**25% d$_{xz}$**		**67% p$_x$**		
25a'	Ru–Cl π	−6.114	12% d$_{yz}$		79% p$_y$		
24a'	Cl–Ru–Sn σ	−6.657	10% 5p$_z$, 7% d$_{z^2}$	30% 3a$_1$	24% p$_z$	15% 2b$_1$	
15a"	Cl–Ru–Sn π	−7.164	39% d$_{xz}$	10% 3e	28% p$_x$	14% 1a$_2$	
23a'	Cl–Ru–Sn π	−7.552	32% d$_{yz}$	39% 3e	12% p$_y$		
22a'	d t$_{2g}$	−7.729	67% d$_{x^2-y^2}$				25% 2π

[a] The HOMO (16a") and LUMO (26a') are printed in bold type.

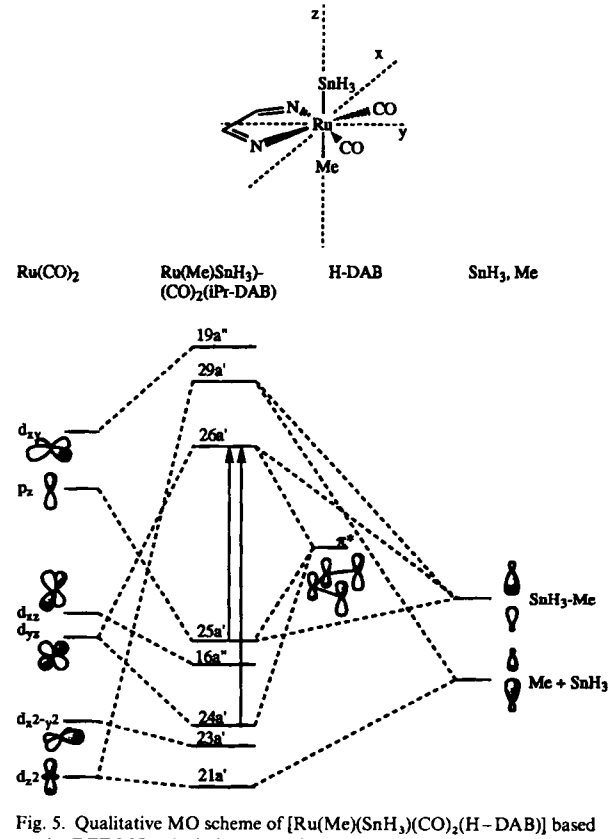

Fig. 5. Qualitative MO scheme of [Ru(Me)(SnH$_3$)(CO)$_2$(H–DAB)] based on the DFT MO calculations; see also Table 3.

Table 2b. Electronic transitions to the lowest ^{1}A' states of [Ru(Cl)(SnH$_3$)(CO)$_2$(H–DAB)]: DFT-calculated changes in Mulliken populations, transition energies and oscillator strengths.

	Ru p$_x$	Ru d$_{z^2}$	Ru d$_{xy}$	Ru d$_{yz}$	DAB a$_1$	DAB b$_1$	DAB b$_2$	CO π	Cl p$_y$	Cl p$_z$	SnH$_3$ a1	SnH$_3$ e	E_S (cm^{-1}) (nm)	E_T (cm^{-1}) (nm)	f_{cal} [a]	f_{exp} [b]
GS	2.31	1.07	0.68	1.57	10.02	2.56	5.64	8.95	1.96	1.58	4.71	12.00				
25a' → 26a'	−0.01	+0.03	+0.04	**−0.17**	−0.07	**+0.32**	−0.06	+0.04	**−0.30**	+0.06	−0.03	0.00	15558 (642)	13579 (736)	0.055	0.052
24a' → 26a'	−0.07	−0.04	+0.04	**+0.12**	−0.10	**+0.36**	−0.06	+0.03	**−0.16**	−0.08	**−0.15**	**+0.03**	17573 (569)	16069 (622)	0.035	
23a' → 26a'	0.00	+0.07	+0.04	**−0.31**	−0.09	**+0.34**	−0.08	−0.14	**−0.11**	+0.06	**+0.09**	**−0.15**	23874 (419)	24897 (402)	0.045	

[a] Oscillator strengths calculated with separately optimised excited state orbitals. [b] Calculated for [Ru(Cl)(SnPh$_3$)(CO)$_2$(*i*Pr–DAB)] from the equation $f = 4.319 \times 10^{-9} \varepsilon_{max} \Delta\tilde{\nu}$ ($\Delta\tilde{\nu}$ = width at half height).

to the axial C–Ru–Sn bonds, originating in the interaction between the antisymmetric sp^3(Sn)–sp^3(Me) combination of the σ orbitals of the axial ligands and the Ru $5p_z$ orbital. Although the Ru(p_z) + (Sn(sp^3)–Me(sp^3)) combination dominates the character of this orbital (overall contribution 61%), also the π*($2b_1$) orbital of the DAB ligand contributes significantly (25%). The situation is reversed for the LUMO, since the contribution from π*($2b_1$) of the DAB ligand dominates (62%) and the Ru(d_{yz}) + (Sn(sp^3)–Me(sp^3)) combination contributes 36%. The same type of σ–π* orbital interaction, to a very similar extent, was calculated for [Ru(SnH_3)$_2$(CO)$_2$(H–DAB)].[31] Apparently, it originates in the simultaneous presence of two strongly σ-donating axial ligands. This σ–π* orbital interaction actually results in an extensive delocalisation by donation of electron density from the Ru(E)(E') moiety into the π system of the DAB ligand. This seems to be the crucial electronic factor responsible for many of the unusual properties of the non-halide class of [Ru(E)(E')(CO)$_2$(*i*Pr–DAB)] complexes. A detailed theoretical study will be published elsewhere.[37]

Assignment of the electronic transitions: The characters of the frontier orbitals and the oscillator strengths *f* (Tables 2b, 3b–c) for the transitions from several of the high-lying MO's to the LUMO derived from the DFT MO calculations on the model complexes were used to interpret the visible absorption and rR spectra of the halide and non-halide complexes, respectively, of the [Ru(E)(E')(CO)$_2$(*i*Pr–DAB)] family.

The halide complexes will be discussed first. For the HOMO → LUMO transition of [Ru(Cl)(SnH_3)(CO)$_2$(H–DAB)], a very small (< 0.0001) oscillator strength was predicted by the calculation, apparently because of a very small overlap between the essentially π*-DAB LUMO and the HOMO that lies in the *xz* plane, not in the direction of the DAB ligand. On the other hand, the 25a' (HOMO-1) orbital is directed toward the DAB ligand. Based on this consideration that is supported by the large calculated *f* value for the model complex, the lowest energy absorption band of [Ru(Cl)($SnPh_3$)(CO)$_2$(*i*Pr–DAB)] and of other halide complexes is attributed to the 25a'(HOMO-1) → 26a'(LUMO) transition. Because of the mixed Ru d(π)–Cl p(π) character of the HOMO-1, a mixed MLCT/XLCT character of the transition is proposed, with the Cl → DAB XLCT contribution prevailing. Of course this description is rather inaccurate because of the delocalised character of the relevant orbitals. This assignment is further supported by the following comparison. The absorption spectrum of [Ru(Cl)($SnPh_3$)(CO)$_2$(*i*Pr–DAB)] closely resembles that of [Ru(Cl)(Me)(CO)$_2$(*i*Pr–DAB)] (see Table 1), and the calculated HOMO-1 characters of the corresponding model complexes are comparable.[37] The oscillator strength of the HOMO-1 → LUMO transition of [Ru(Cl)(Me)(CO)$_2$(H–DAB)] was calculated as 0.041,[37] and that of the same transition of [Ru(Cl)(SnH_3)(CO)$_2$(H–DAB)] as 0.055 (see Table 2b). The ratio between these oscillator strengths (1.34) is in agreement with that between the peak areas of the lowest energy absorption bands of [Ru(Cl)(Me)(CO)$_2$(*i*Pr–DAB)] and [Ru(Cl)($SnPh_3$)(CO)$_2$(*i*Pr–DAB)] (1.66).

The predominant Ru/Cl- and DAB-localised characters of the HOMO-1 and LUMO, respectively, suggest a rather localised character of the MLCT/XLCT transitions, in full accord with the rR spectral patterns exhibited by all the halide complexes studied (vide supra). These species also consistently show a rather large solvatochromism.

For the non-halide model complex [Ru(Me)(SnH_3)(CO)$_2$(H–DAB)] the 25a' HOMO and 26a' LUMO are of the same symmetry, both consisting essentially of the same atomic or fragment orbitals (see Table 3). Accordingly, the calculated oscillator strengths of the HOMO → LUMO transitions of both [Ru(Me)(SnH_3)(CO)$_2$(H–DAB)] and [Ru(SnH_3)$_2$(CO)$_2$(H–DAB)][31] are quite large. Hence, we assign the lowest absorption band in the spectra of the non-halide complexes to this HOMO → LUMO transition, which can best be viewed as a $\sigma_{E-Ru-E'} \rightarrow \pi^*_{DAB}$ (= σ → π*) transition, since the HOMO has σ character with respect

Table 3a. DFT-calculated characters (%) and energies of the MO's of [Ru(Me)(SnH_3)(CO)$_2$(H–DAB)] [a].

Orbital	Description	ε (eV)	Ru	SnH_3	Me	H–DAB	CO
26a'	**DAB π***	**−3.981**	**10% d_{yz}**	**15% $3a_1$**	**11% $2a_1$**	**62% $2b_1$**	
25a'	**Me–Ru–Sn σ**	**−5.812**	**13% p_z**	**28% $3a_1$**	**20% $2a_1$**	**25% $2b_1$**	
16a''	d t_{2g}	−6.179	67% d_{xz}	5% 3e		11% $1a_2$	10% 2π
24a'	d t_{2g}	−6.717	60% d_{yz}	12% 3e	4% 1e	12% $2b_1$	11% 2π
23a'	d t_{2g}	−7.208	68% $d_{x^2-y^2}$				26% 2π

[a] The HOMO (25a') and LUMO (26a') orbitals are printed in bold type.

Table 3b. Electronic transitions to the lowest ^{1}A' states of [Ru(Me)(SnH_3)(CO)$_2$(H–DAB)]: DFT-calculated changes in Mulliken populations, transition energies and oscillator strengths.

	Ru p_z	Ru d_{z^2}	Ru d_{xy}	Ru d_{yz}	DAB a_1	DAB b_1	DAB b_2	CO π	SnH_3 a1	SnH_3 e	Me a1	Me e	E_S (cm^{-1}) (nm)	E_T (cm^{-1}) (nm)	f_{cal} [a]	f_{exp} [b]
GS	2.31	1.06	0.68	1.57	10.02	2.75	7.66	9.03	4.75	12.01	3.22	4.01				
25a' → 26a'	**−0.13**	−0.01	0.00	**+0.08**	−0.06	**+0.24**	−0.06	−0.03	**−0.09**	0.00	−0.05	0.03	16914 (591)	13419 (745)	0.105	0.054
24a' → 26a'	**+0.03**	+0.08	+0.04	**−0.38**	−0.06	**+0.36**	−0.10	−0.09	**+0.14**	−0.17	+0.08	0.07	24460 (409)	23362 (428)	0.023	

[a] Oscillator strengths calculated with separately optimised excited-state orbitals. [b] Calculated for [Ru(Me)($SnPh_3$)(CO)$_2$(*i*Pr–DAB)] from the equation $f = 4.319 \times 10^{-9} \varepsilon_{max} \Delta\tilde{\nu}$ ($\Delta\tilde{\nu}$ = width at half height).

Table 3c. Electronic transitions to the lowest ^{1}A' states of [Ru(SnH_3)$_2$(CO)$_2$(H–DAB)]: DFT-calculated changes in Mulliken populations, transition energies and oscillator strengths.

	Ru p_z	Ru d_{z^2}	Ru d_{xy}	Ru d_{yz}	DAB a_1	DAB b_1	DAB b_2	CO π	SnH_3 a	SnH_3 e	E_S (cm^{-1}) (nm)	E_T (cm^{-1}) (nm)	f_{cal} [a]	f_{exp} [b]
GS	2.49	1.23	0.70	1.60	10.00	2.77	7.63	9.66	9.44	24.01				
10b1 → 11b1	**−0.13**	−0.02	+0.02	**+0.07**	−0.06	**+0.20**	−0.04	−0.06	**−0.09**	**−0.01**	17524 (571)	14408 (694)	0.122	0.057
9b1 → 11b1	**+0.02**	+0.07	+0.05	**−0.33**	−0.06	**+0.37**	−0.09	−0.10	**+0.27**	**−0.29**	26607 (376)	25412 (394)	0.010	

[a] Oscillator strengths calculated with separately optimised excited-state orbitals. [b] Calculated for [Ru($SnPh_3$)$_2$(CO)$_2$(*i*Pr–DAB)] with the equation $f = 4.319 \times 10^{-9} \varepsilon_{max} \Delta\tilde{\nu}$ ($\Delta\tilde{\nu}$ = width at half height).

0947-6539/96/0212-1560 $ 15.00+.25/0 Chem. Eur. J. 1996, 2, No. 12

to the axial bonds and the LUMO is mostly of π*-DAB origin (vide supra).

Indeed, the changes in the population densities calculated for [Ru(SnH$_3$)$_2$(CO)$_2$(H–DAB)] (Table 3c) and [Ru(Me)(SnH$_3$)(CO)$_2$(H–DAB)] (Table 3b) show that the only significantly depopulated orbitals are Ru p_z and Sn a_1, and Me a_1 in the latter complex, while the population of the π*-DAB orbital increases. The overall charge separation is smaller than that calculated for [Ru(Cl)(SnH$_3$)(CO)$_2$(H–DAB)], because of an extensive σ–π* delocalisation in the former, non-halide, complexes. This latter factor is responsible for the small solvatochromic effect and it also diminishes the structural effects of the σ → π* excitation, distributing them over many normal coordinates, as indicated by the rR spectra.

Excited state properties: All complexes studied show, in a 2-MeTHF glass at 80 K, an intense unstructured emission band upon excitation into their lowest energy absorption band. The emission data obtained at 460 and 532 nm excitation are collected in Table 4. In all cases studied, the excited-state lifetimes are essentially determined by the rate of the nonradiative decay, since k_{nr} is always much larger than the rate constant for the radiative decay, k_r (see Table 4). As can be seen from Table 4, there is a clear distinction between the two classes of [Ru(E)(E′)(CO)$_2$(*i*Pr–DAB)] complexes. Thus, compared with the values of the non-halide complexes, the halide complexes show the emission band at higher energy, the apparent Stokes shift (ΔE_{abs-em}) and rate constant for nonradiative decay (k_{nr}) are larger, and the lifetimes of the excited states are shorter. All these data indicate that we are dealing with quite different types of excited states for the two classes. We will therefore discuss them in separate sections, focussing on the differences within the groups of complexes.

[Ru(Cl)(E′)(CO)$_2$(iPr–DAB)] (E′ = SnPh$_3$, PbPh$_3$): Figure 6 shows the absorption, emission and excitation spectra of [Ru(Cl)(SnPh$_3$)(CO)$_2$(*i*Pr–DAB)] in a 2-MeTHF glass at 80 K. The excitation spectrum measured for the emission at 650 nm exactly matches the ground-state absorption spectrum, indicating that the emitting state is populated from the optically excited

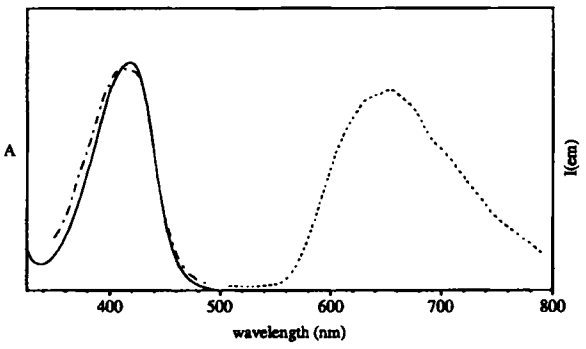

Fig. 6. Absorption spectrum (—), excitation spectrum (λ_{em} = 650 nm) (·····); emission spectrum (λ_{exc} = 424 nm) (- - -) of [Ru(Cl)(SnPh$_3$)(CO)$_2$(*i*Pr–DAB)] in a 2-MeTHF glass at 80 K.

state with a constant efficiency, independent of the excitation wavelength.

Comparing the data for the three halide complexes (E = Cl, E′ = Me, SnPh$_3$, PbPh$_3$) we see that the ground-state absorption band shifts from 387 to 427 nm while the emission wavelength decreases from 650 to 634 nm. The resulting decrease of the apparent Stokes shift on going from [Ru(Cl)(Me)(CO)$_2$(*i*Pr–DAB)] to [Ru(Cl)(SnPh$_3$)(CO)$_2$(*i*Pr–DAB)] and [Ru(Cl)(PbPh$_3$)(CO)$_2$(*i*Pr–DAB)] indicates that the excited-state distortion decreases in the same order. The excited-state lifetime increases with decreasing apparent Stokes shift, while the emission energy changes only little. As in previous cases,[2, 5, 28] such a behaviour may indicate an increase of Cl → DAB XLCT character of the emitting CT excited state. Indeed, this explanation is supported by the calculated changes in orbital population on the HOMO-1 → LUMO (MLCT/XLCT) excitation, which show that, for [Ru(Cl)(Me)(CO)$_2$(H–DAB)], the electron density in the Ru d_{yz} and Cl p_y orbitals change by −0.32 and −0.21, respectively,[37] while values of −0.17 and −0.30 are obtained for [Ru(Cl)(SnH$_3$)(CO)$_2$(H–DAB)]. Population of the π* ($2b_1$) DAB orbital was calculated for these complexes to increase by +0.42 for [Ru(Cl)(Me)(CO)(H–DAB)] and +0.32 for [Ru(Cl)(SnH$_3$)(CO)$_2$(H–DAB)], showing that the CT transition is indeed directed to the DAB ligand.

Table 4. Emission properties of the [Ru(E)(E′)(CO)$_2$(*i*Pr–DAB)] complexes in a 2-MeTHF glass (80 K).

Compound E	E′	λ_{abs} (nm)	λ_{exc} = 460 nm λ_{em} (nm)	Stokes shift ΔE (cm^{-1}) [a]	τ (μs)	Φ_r (×10^{-4})	k_r (s^{-1})	k_{nr} (×10^4 s^{-1})	λ_{exc} = 532 nm λ_{em} (nm)	Stokes shift ΔE (cm^{-1}) [a]	τ (μs)
Cl	Me [b]	387	650	10455	0.3	3.4	1140	384.4			
I	Me [b]	410	642	8814	1.8	37	2100	55			
Cl	SnPh$_3$	420	637	8111	7.36	13.4	182	13.7			
Cl	PbPh$_3$	427	634	7646	≈10	≈11.6	≈116	≈10			
SnPh$_3$	SnPh$_3$	495	670	5277	264	146	55	0.37	708	6078	125
			543	1786	<0.01	–	–	–			
SnPh$_3$	SnMe$_3$	500	694	5591	160	32	20	0.62	720	6111	96
SnPh$_3$	GePh$_3$	505	693	5372	178	25	14	0.56	720	5913	109
			559	1913	<0.01	–	–	–			
Me	SnPh$_3$	501	715	5974	31	10	32	3.19	750	6628	20
			578	2659	<0.01	–	–	–			
PbPh$_3$	PbPh$_3$	518	690	4812	74	–	–	–	690	4812	≈74 [d]
									≈710	5221	≈68 [d]
PbPh$_3$	PbMe$_3$	532	≈682	4653	62 [d]	4	–	–	≈682	4653	≈62 [d]
			≈707	4908	39 [d]				≈707	4908	≈39 [d]
PbPh$_3$	GePh$_3$	515	700	5132	36	16	44	2.8	720	5529	44
Me [c]	PbPh$_3$	510	702	5363	≈24	≈3	≈12	≈4.2	720	5719	
SnPh$_3$	CO [e]	451	687	7424	13	8	6	7.6			
SnPh$_3$	CO [f]	447	642	6795	26	8	29	3.9			

[a] Apparent Stokes shift defined as $\Delta E = E_{abs} - E_{em}$. [b] From ref. [2]. [c] No accurate lifetime measured owing to partial photodecomposition. [d] Two overlapping signals with different lifetimes. [e] [Re(SnPh$_3$)(CO)$_3$(*i*Pr–DAB)] from ref [41]. [f] [Re(SnPh$_3$)(CO)$_3$(*i*Pr–PyCa)] from ref. [41].

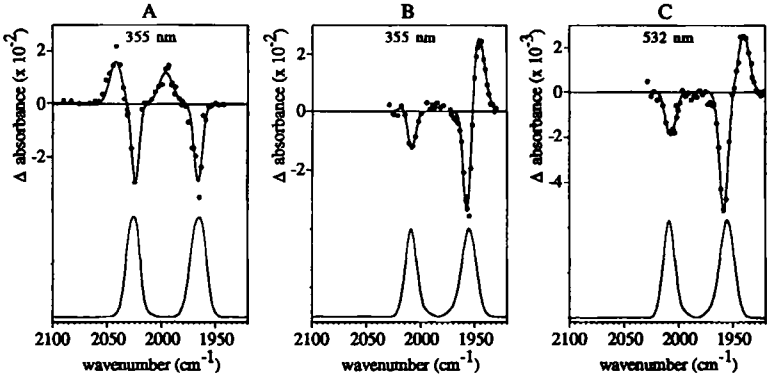

Fig. 7. TRIR (top) and FTIR (bottom) spectra of [Ru(Cl)(SnPh$_3$)(CO)$_2$(*i*Pr-DAB)] (**A**) and [Ru(SnPh$_3$)$_2$(CO)$_2$(*i*Pr-DAB)] (**B**, **C**), all at 77 K in *n*PrCN. The TRIR spectra were obtained 120 ns after laser excitation. Each point corresponds to a different line of the IR diode laser; points below the zero line depict loss of the parent, while those above the line indicate the generation of a new species.

Time-resolved (ns timescale) infrared (TRIR) spectra afforded information on the degree of charge transfer upon excitation, since the position of the ν(CO) bands is sensitive to the oxidation state of the metal.[38] The changing XLCT/MLCT character of the emitting excited state is also confirmed in the TRIR spectra of the halide complexes at room temperature or in a *n*PrCN glass at 77 K (Fig. 7 and Table 5). The TRIR spectrum of [Ru(Cl)(SnPh$_3$)(CO)$_2$(*i*Pr-DAB)] at 77 K measured $\approx$120 ns after excitation shows bleaching of the ground-state absorption and formation of new transient peaks at 2051 and 2003 cm^{-1}. These transient peaks are shifted by 18 and 29 cm^{-1}, respectively, to higher wavenumbers relative to the ground-state ones. Identical shifts were observed at room temperature. The intensities of the IR transient absorption peaks as well as of the bleach decayed with a lifetime of 7.6 μs, comparable to the emission lifetime of 7.4 μs measured in 2-MeTHF at 77 K. Hence, the transient IR absorption is assigned to the emitting excited state. When compared with the TRIR spectra of [Ru(Cl)(Me)(CO)$_2$(*i*Pr-DAB)] and [Ru(I)(Me)(CO)$_2$(*i*Pr-DAB)] studied earlier,[5] the positive shifts in wavenumber of both bands, $\Delta\tilde{\nu}$, and the increase of the CO stretching force constant, Δk, on excitation decrease in the order [Ru(Cl)(Me)(CO)$_2$(*i*Pr-DAB)] > [Ru(I)(Me)(CO)$_2$(*i*Pr-DAB)] > [Ru(Cl)(SnPh$_3$)(CO)$_2$(*i*Pr-DAB)], which reflects the diminishing effect of the excitation on the Ru → CO π back donation (see Table 5). As mentioned above, this trend may be explained by an increase of XLCT character of the emitting state.[2, 5]

The time-resolved UV/vis absorption spectrum of [Ru(Cl)(SnPh$_3$)(CO)$_2$(*i*Pr-DAB)] obtained in THF at room temperature at 10 ns after the 532 nm excitation pulse (Fig. 8) shows a bleached ground-state absorption and a transient absorption that consists of a weak, broad band around 500 nm and a strong maximum at about 350 nm. All these features decay with a lifetime of $\approx$1 μs, that is, one comparable to the emission lifetime of 1.1 μs at 293 K; this justifies their assignment to the emitting excited state.

The complex [Ru(Cl)(SnPh$_3$)(CO)$_2$(*i*Pr-DAB)] and its congeners[12] [Ru(Cl)(Me)(CO)$_2$(*i*Pr-DAB)] and [Ru(I)(Me)(CO)$_2$(*i*Pr-DAB)] show a strongly temperature-dependent emission lifetime in fluid solution, whose analysis may provide information on the mechanism of the nonradiative excited state decay.[25, 39] The experimental data fit Equation (1) well;

$$1/\tau = k_0 + A\exp(-E_a/RT) \quad (1)$$

$k_0 = 2.4\times10^5\ s^{-1}$, $A = 1.1\times10^8\ s^{-1}$, $E_a = 1009\pm20\ cm^{-1}$, $r^2 = 0.999$. Compared with the I → DAB (XLCT) excited complex [Ru(I)(Me)(CO)$_2$(*i*Pr-DAB)}],[12] the value of k_0, which

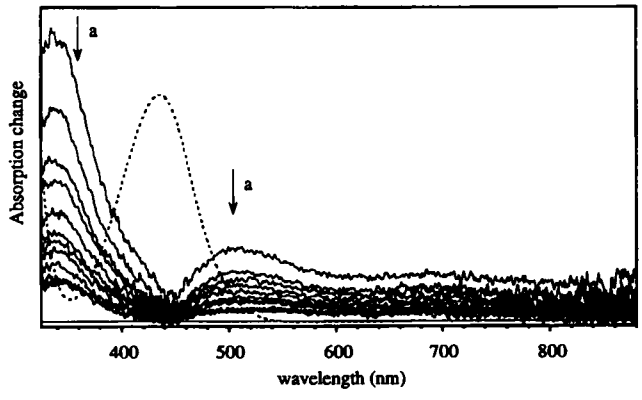

Fig. 8. UV/vis time-resolved absorption spectra of [Ru(Cl)(SnPh$_3$)(CO)$_2$(*i*Pr-DAB)] in THF at room temperature, (λ_{exc} = 460 nm, 12 mW pulse^{-1}; delay between the spectra 200 ns; lifetime of the transient $\approx$1 μs).

Table 5. TRIR data for [Ru(E)(E')(CO)$_2$(*i*Pr-DAB)] complexes.

Compound E	Compound E'	state [a]	λ_{exc} (nm)	T (K)	ν_s (cm^{-1})	ν_{as} (cm^{-1})	k [b] (Nm^{-1})	k_i [b] (Nm^{-1})	τ (μs)	$\Delta\tilde{\nu}$ [c] (cm^{-1})	Δk [d] (Nm^{-1})
Cl [e]	Me	G. S.	355	293	2030	1962	1611	54.8	[f]		
		E. S.			2081	2014	1693	55.4	[f]	51/52	82
I [e]	Me	G. S.	355	293	2031	1967	1614	51.7	0.23		
		E. S.			2058	2010	1671	39.4	0.25	27/43	57
I [e]	Me	G. S.	532	293	2033	1964			0.21		
		E. S.			2057	2006	1667	41.8	0.22	24/42	53
Cl [g]	$SnPh_3$	G. S.	355	293	2034	1973	1621	49.4			
		E. S.			2051	2003	1659	39.3	0.7	17/30	38
Cl [h]	$SnPh_3$	G. S.	355	77	2024	1966	1608	46.7	7.6		
		E. S.			2042	1995	1646	38.3	7.6	18/29	38
$SnPh_3$ [h]	$SnPh_3$	G. S.	355	77	2006	1955	1579	35.9	250 [i]		
		E. S.			$\approx$2006	1944	1571	44.6	250 [i]	$\approx$0/$\approx$ −11	−8
$SnPh_3$ [h]	$SnPh_3$	G. S.	532	77	2006	1955	1579	35.9	90 [j]		
		E. S.			$\approx$2006	1940	1568	47.7	90 [j]	$\approx$0/$\approx$ −15	−11

[a] G. S. = ground state; E. S. = excited state. [b] k (= force constant) and k_i (= interaction force constant) calculated with formulae from ref. [63]. [c] $\Delta\tilde{\nu} = \tilde{\nu}_{s(excited\ state)} - \tilde{\nu}_{s(ground\ state)}$ and $\tilde{\nu}_{as(excited\ state)} - \tilde{\nu}_{as(ground\ state)}$. [d] $\Delta k = k_{(excited\ state)} - k_{(ground\ state)}$. [e] In CH_2Cl_2, from ref. [5]. [f] Trace too noisy to obtain accurate kinetic fit. [g] In CH_2Cl_2. [h] In *n*PrCN. [i] Lifetimes obtained with sample concentration 10^{-4} M. [j] Lifetimes obtained with sample concentration 10^{-3} M.

0947-6539/96/0212-1562 $ 15.00+.25/0 Chem. Eur. J. 1996, 2, No. 12

reflects the rate of the intrinsic nonradiative deactivation[25, 39] through the weak coupling with the ground state, is about 7.5 times lower for [Ru(Cl)(SnPh$_3$)(CO)$_2$(*i*Pr–DAB)]. This is in accordance with the smaller distortion of this latter complex in its XLCT/MLCT-excited state, which is manifested by the smaller apparent Stokes shift. The thermally activated pathway appears to involve deactivation by an unidentified higher-lying excited state. The activation barrier is somewhat higher than that found for [Ru(I)(Me)(CO)$_2$(*i*Pr–DAB)] (610 cm^{-1}).[2]

In conclusion, the experimental data indicate a mixed ^{3}(MLCT/XLCT) character of the emitting excited state for all the halide complexes studied. This assignment is further supported by the results of the DFT calculations on the [Ru(Cl)(SnH$_3$)(CO)$_2$(H–DAB)] model complex.

[Ru(E)(E')(CO)$_2$(iPr–DAB)] (E, E' ≠ halide): Figure 9 shows the absorption, emission and excitation spectra measured in 2-MeTHF glass at 80 K of [Ru(SnPh$_3$)$_2$(CO)$_2$(*i*Pr–DAB)], which is a representative of the non-halide complexes.

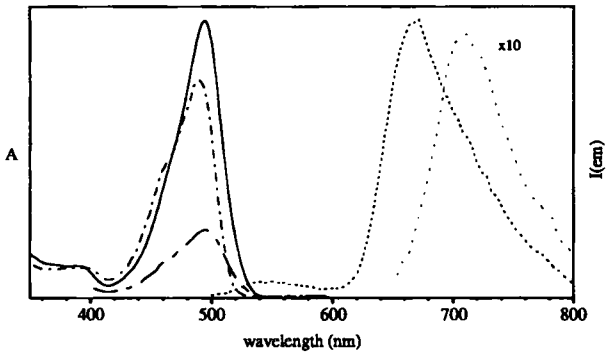

Fig. 9. Absorption spectrum (—); emission spectra (λ_{exc} = 460 nm (···) and λ_{exc} = 525 nm (· · ·)); excitation spectra (λ_{em} = 750 nm (– – –) and λ_{em} = 650 nm (– · – · –)) of [Ru(SnPh$_3$)$_2$(CO)$_2$(*i*Pr–DAB)] in a 2-MeTHF glass at 80 K.

At 80 K, this species exhibits three emissions depending on the excitation wavelength used. Excitation at the high-energy side (460 nm) of the absorption band (λ_{max} = 495 nm) gives rise to an intense long-lived (264 μs) emission appearing at 670 nm and to a very short-lived (< 10 ns) emission at 543 nm. Excitation at 532 nm at the low-energy side of the absorption band produces a much weaker emission at 708 nm with a lifetime of 125 μs. Similar behaviour was observed for other non-halide complexes and relevant emission data are listed in Table 4. The very short-lived high energy emission was found only for some of the complexes studied. Based on the very short lifetime and very small Stokes shift, it was assigned tentatively to the $^1\sigma\pi^*$ state and not studied further. Figure 9 shows the excitation spectra measured for the 670 and 708 nm emissions of [Ru(SnPh$_3$)$_2$(CO)$_2$(*i*Pr–DAB)], respectively. Obviously, the two emissions originate in two different excitations hidden within the absorption band envelope. The excitation band corresponding to the stronger, longer-lived, 670 nm emission is more intense and lies at somewhat higher energy than that corresponding to the 708 nm emission.

Comparing these data with the low-temperature absorption spectrum of [Ru(SnPh$_3$)$_2$(CO)$_2$(*i*Pr–DAB)] (vide supra), we see that the asymmetry in the absorption band is related to the presence of two maxima in the excitation spectra and the appearance of two emissions. In principle these two emissions might belong to two different excited states of the same complex, or to molecules located at different sites in the glass,[40] or to different conformers. The first possibility is rather unlikely, since the second allowed electronic transition of this complex is expected at higher energy and it has an MLCT character.[31] A much shorter lifetime is expected for such an MLCT state. Emission from two complexes at different sites cannot be excluded here. However, in view of the fact that the small splitting of the ν_s(CN) band in the IR and Raman spectra indicates the presence of two conformers, we tentatively assign the two emissions to such species.

The lifetimes of the two emissions could only be determined accurately for complexes having their low-energy absorption band in between the two laser lines available (460 and 532 nm). This is the case for most of the tin-containing complexes, for which the absorption band maxima lie between 495 and 505 nm. The absorption bands of the lead complexes are red-shifted to between 510 and 532 nm, and the excitation at 532 nm populates both emissive states; only an estimate could be made with respect to the lifetime of the high-energy emission.

Values of the apparent Stokes shift measured for the main long-lived emission of the non-halide complexes (Table 4) are much smaller than those reported previously for either ^{3}MLCT or ^{3}XLCT emissions from Ru or Re carbonyl–diimine complexes.[2, 28] These features, together with the $\sigma \rightarrow \pi^*$ nature of the lowest electronic transition as derived from DFT calculations, clearly show[2, 27, 41, 42] that the emitting lowest excited state has a $^3\sigma\pi^*$ character. The small Stokes shift values indicate a very small molecular distortion that is typical for $^3\sigma\pi^*$ excited states.[2, 27, 41, 42] This distortion should be minimal for the most delocalised systems, in which there is efficient compensation for the differences in charge distribution between the ground and excited states. As can be seen from Table 4, the excited state distortion is the smallest and, hence, the delocalisation presumably the largest for the symmetrically substituted complexes [Ru(EPh$_3$)$_2$(CO)$_2$(*i*Pr–DAB)] (E = Sn, Pb) and apparently decreases for complexes in which the two axial ligands differ. This trend is corroborated by the emission data obtained from 532 nm excitation.

The lifetimes of the main $\sigma\pi^*$ emission of the non-halide complexes show large variations with the actual complex composition, even with the substituents at the Pb or Sn donor atoms (EPh$_3$ or EMe$_3$). Within the group of the Sn-containing complexes the decrease of the lifetime of the main emission band (670 nm) qualitatively correlates with the decrease of the emission energy and increase of the Stokes shift, although the variations of the latter two parameters are not large. In general, the lifetimes obtained with 532 nm excitation follow the same trends.

The time-resolved UV/vis absorption spectrum of [Ru(SnPh$_3$)$_2$(CO)$_2$(*i*Pr–DAB)] obtained in THF 10 ns after the 532 nm excitation pulse at room temperature (Fig. 10) has a bleached ground-state absorption and a transient absorption that consists of intense bands at 590 and 350 nm. All these features decay with a lifetime of ≈1 μs, justifying their assignment to the emitting excited state, which has the same lifetime at 290 K. The presence of a strong absorption at 590 nm, slightly red-shifted from the ground state absorption band, is consistent with the proposed $^3\sigma\pi^*$ character of the excited state studied. A similar feature was found for the $^3\sigma\pi^*$ excited states of [Re(Bz)(CO)$_3$(*i*Pr–DAB)][27] and [Re(SnPh$_3$)(CO)$_3$(α-diimine)][42] in toluene.

The $\sigma\pi^*$ character and small distortion of the excited state is also demonstrated by the TRIR spectrum of the [Ru(SnPh$_3$)$_2$(CO)$_2$(*i*Pr–DAB)] complex at 77 K in a PrCN glass (see Fig. 7). The spectrum measured at ≈120 ns after the 355 nm laser excitation shows bleaching of the ground-state absorption bands at

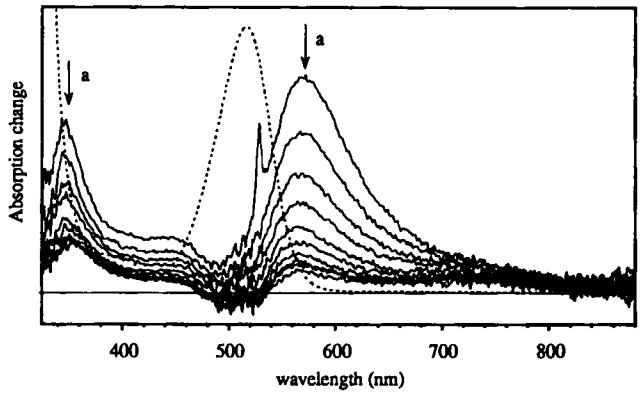

Fig. 10. UV/vis time-resolved absorption spectra of $[Ru(SnPh_3)_2(CO)_2(iPr-DAB)]$ in THF at room temperature. (λ_{exc} = 532 nm, 80 mW pulse^{-1}; delay between the spectra 300 ns; lifetime of the transient $\approx$1 μs).

2006 and 1955 cm^{-1}. The bleach of the band at about 2006 cm^{-1} is less intense because of the overlap with a transient absorption peak arising at approximately the same position. A well-developed transient peak appears at 1944 cm^{-1}, its formation being completed within the 50 ns instrumental risetime. The lifetime of 250 μs calculated from the TRIR decay traces at 1955 and 1944 cm^{-1} is in accordance with the results obtained from emission spectroscopy, with a comparable sample concentration of $\approx 10^{-4}$ M. The excited-state decay is concomitant with the recovery of the ground state absorption. The TRIR spectra measured after the 532 nm excitation again showed a transient peak at 1940 cm^{-1}, close to the value of 1944 cm^{-1} measured after the 355 nm excitation. Unfortunately, the 532 nm excited TRIR spectra could only be measured for the complex at a higher concentration (ca. 10^{-3} M) than that used for the emission experiments. This caused a decrease in the lifetime, since the lifetime was 125 μs as derived from the emission spectra (10^{-4} M) but only 90 μs according to the TRIR data (10^{-3} M). In order to confirm this concentration effect, emission lifetimes were determined after 355, 460 and 532 nm excitation of a 5×10^{-4} M solution of the complex in a BuCN/PrCN (5:4, v:v) glass at 80 K. Excitation with 355 or 460 nm caused emission at 680 nm, decaying with a lifetime of 180 μs (264 μs at 10^{-4} M, see Table 4). Upon excitation with 532 nm light, the emission lifetime was 110 μs, in between the values obtained at 10^{-4} M in emission (125 μs, see Table 4) and at 10^{-3} M in TRIR (90 μs, see Table 5). The close correspondence between the 355 and 532 nm excited TRIR spectra supports our assumption that the transients which appear after the 355/460 nm and 532 nm excitations, respectively, belong to two conformers.

All these results indicate that the transient may be assigned to the emissive excited state. Assuming that the high wavenumber IR peak at 2006 cm^{-1} hardly shifts on excitation with 355 nm, the shift of the lower one at 1955 cm^{-1} by -11 cm^{-1} indicates a decrease of the CO stretching force constant (Δk) by 8 Nm^{-1}. This clearly shows that the emitting excited state has neither MLCT nor XLCT character, for which large positive shifts of the wavenumbers of the CO stretching vibrations and increases in the corresponding force constants have always been observed.[5] However, a zero or slightly negative shift of the average ν(CO) wavenumbers has already been observed for the $\sigma\pi^*$-excited $[Re(Bz)(CO)_3(iPr-DAB)]$ complex.[27,42] The TRIR spectrum of $[Ru(SnPh_3)_2(CO)_2(iPr-DAB)]$ thus further supports the assignment of the emitting excited state to the $^3\sigma\pi^*$ state.

The mechanism of the nonradiative decay of the $^3\sigma\pi^*$ excited state of $[Ru(SnPh_3)_2(CO)_2(iPr-DAB)$ was investigated by following the emission lifetime of this complex in fluid THF as a function of the temperature. Only a single, relatively broad, emission band at $\approx$780 nm was observed. The emission lifetime in solution does not depend on the excitation wavelength (460 or 532 nm). The temperature dependence of the excited-state lifetime again follows Equation (1), with the parameters $k_0 = 3.1 \times 10^4$ s^{-1}, $A = 3.9 \times 10^8$ s^{-1}, $E_a = 1470 \pm 70$ cm^{-1} and $r^2 = 0.988$. The k_0 value is nearly 8 times smaller than that for the XLCT/MLCT state of $[Ru(Cl)(SnPh_3)(CO)_2(iPr-DAB)]$ and $\approx$10–100 times smaller than the values typically encountered for ^{3}MLCT states of $[Ru(bpy)]^{2+}$-type complexes[39] or $[Re(Cl)(CO)_3(bpy)]$.[25] Such a very slow intrinsic rate of the nonradiative transition (i.e. tunnelling) to the ground state appears to be one of the salient features of the $^3\sigma\pi^*$ excited states.[27,42,43] The thermally activated pathway involves a somewhat larger barrier than for the $[Ru(Cl)(SnPh_3)(CO)_2(iPr-DAB)]$ complex. Most probably, it corresponds to a thermally activated population of a chemically reactive excited state, as will be discussed elsewhere.[44]

Conclusion

The "halide" and "non-halide" classes of $[Ru(E)(E')(CO)_2(iPr-DAB)]$ complexes differ appreciably in their ground- and excited-state properties. Both the lowest electronic transition and excited state of the halide complexes $[Ru(Cl)(E')(CO)_2(iPr-DAB)]$ have mixed MLCT/XLCT character, which changes appreciably on variation of E'. The simultaneous presence of two σ-bonded ligands in the axial positions gives rise to a $\sigma_{(E-Ru-E')} \rightarrow \pi^*_{DAB}$ lowest-energy electronic transition. Extensive delocalisation between the axial Ru(E)(E') moiety and the π* system of the DAB ligand exists both in the ground and excited states. Consequently, the $\sigma \rightarrow \pi^*$ excitation occurs with unusually large oscillator strength and the $^3\sigma\pi^*$ lowest excited state is only a little distorted relative to the ground state. Hence the $^3\sigma\pi^*$ excited states have exceptionally long lifetimes. These properties are most pronounced in complexes with identical or similar E and E' axial ligands, for example $[Ru(SnPh_3)_2(CO)_2(iPr-DAB)]$.

These results clearly show that the introduction of two σ-bonded ligands into diimine complexes opens a route to a new class of photoactive compounds with strongly emitting, long-lived excited states.

Experimental Section

Materials and preparation: Solvents were freshly distilled from sodium wire (THF (p.a.), 2-MeTHF (p.a.), hexane (p.a.)) or CaH_2 (propionitrile and butyronitrile) and handled under a N_2 atmosphere. The syntheses, structures and spectroscopic properties (^{1}H, ^{13}C NMR, IR, UV/vis) of the complexes studied have been described elsewhere [29,31].

Spectroscopic measurements: Electronic absorption spectra were recorded on a Varian Cary 4E spectrophotometer. IR spectra were obtained on a BioRad FTS-A60 FTIR spectrometer equipped with a liquid nitrogen cooled MCT detector. Resonance Raman spectra of the samples, prepared as KNO_3 pellets, were measured on a Dilor XY spectrometer with a multichannel diode array detection system. A Spectra Physics 2016 Ar^+ laser was used as excitation source. To avoid photodecomposition during the Raman measurement the pellet was kept spinning and the exciting laser beam was directed onto it through a rotating prism. The Raman spectra were corrected for the emission of the complexes and recalibrated for the excitation-wavelength-dependent diode-array shift by means of Grams software [45]. Emission and excitation spectra were measured with a Spex Fluorolog II emission spectrometer with a RCA-C31034 GaAs photomultiplier. The samples used for emission spectroscopy were dissolved in freshly distilled 2-MeTHF, freeze-pump-thaw degassed, and sealed off under vacuum in a cylindrical cuvette (diameter 1 cm). The concentration was chosen such that the maximum absorbance in the

0947-6539/96/0212-1564 $ 15.00+.25/0 Chem. Eur. J. 1996, 2, No. 12

spectral region investigated did not exceed 0.2. Low-temperature UV/vis and IR measurements were carried out in an Oxford Instruments DN1704/54 liquid nitrogen cryostat, equipped with NaCl, CaF_2 or quartz windows.

Time-resolved spectroscopy: The detailed experimental setup for the time-resolved emission and absorption measurements has been described elsewhere [28]. Low-temperature measurements (77 K) in 2-MeTHF glasses were performed in an Oxford Instruments DN1704/54 liquid nitrogen cryostat. For time-resolved absorption spectroscopy of photolabile complexes a homebuilt computer-controlled (OMA) stopped-flow cell was used [28]. Emission lifetimes (τ) were determined from the spectra measured at 20 progressive delay times (t) by fitting the decay of the emission intensity (I) at a minimum of 10 different wavelengths of the emission band to first-order kinetics ($I_t = I_0 \exp(-t/\tau)$) [45]. Emission quantum yields (Φ_{em}) were measured relative to a standard solution of [Re(Cl)(CO)$_3$(bpy)]; solutions with an absorbance <0.2 at 460 nm were used [25]. The necessary corrections were applied [24,46]. All calculations on the spectra (determination of τ, Φ_{em}, etc.) were performed with Grams software [45].

The time-resolved IR (TRIR) spectra were recorded [5,47] at the University of Nottingham (U. K.). The 355 or 532 nm line (pulse width 7 ns) of a Quanta-Ray GCR-12S Nd:YAG laser was used to excite the sample. An infrared diode laser (Mütek MDS 1100) was used as an IR probe. It was tuned between 1880 and 2040 cm^{-1}. The changes in IR absorption at a selected wavenumber were monitored with a photovoltaic 77 K MCT detector (Laser Monitoring Systems PV 2180) having a risetime of ≈ 50 ns. The kinetic traces obtained at different wavenumbers were used to construct the transient IR spectra point by point at given time delays. The sample solution (CH_2Cl_2) flowed through the IR cell after each laser flash. Low-temperature TRIR measurements (77 K) in *n*PrCN glasses were performed in a homebuilt cryostat [48].

Computational details: All DFT MO calculations were performed with the Amsterdam Density Functional program package ADF [49,50]. The computational scheme is characterised by the use of a density-fitting procedure to obtain accurate Coulomb and exchange potentials in each SCF cycle, by the accurate and efficient numerical integration of the Hamiltonian matrix elements [51,52] and the possibility of freezing core orbitals. The LSD exchange correlation potential was used [53] with Vosko–Wilk–Nusair [54] parametrisation of the electron gas data for the local density approximation of the correlation energy. Becke's nonlocal corrections [55,56] to the exchange energy and Perdew's non-local corrections [57,58] to the correlation energy were used. A double-ζ STO basis set for H, C, N and O was used, and a triple-ζ STO basis set for Ru and Sn was employed. The calculations will be referred to throughout this paper as "DFT MO calculations" since the Kohn–Sham formulation of density functional theory leads to molecular orbitals with a good physical basis that can be used very well in MO theoretical considerations [59]. All bases were augmented with one polarisation function. Transition dipole moments were calculated by the program Dipole with separately optimised excited-state orbitals [60].

The structural parameters used for the DFT MO calculations of [Ru(Cl)(SnH$_3$)(CO)$_2$(H–DAB)] were based on the crystal structure of [Ru(Cl)(SnPh$_3$)(CO)$_2$(*i*Pr–DAB)] [29], and those used for [Ru(Me)(SnH$_3$)(CO)$_2$(H–DAB)] were based on the crystal structures of [Ru(SnPh$_3$)$_2$(CO)$_2$(*i*Pr–DAB)] [31] and [Ru(Me){Mn(CO)$_5$}(CO)$_2$(*i*Pr–PyCa)] [3]. To increase the speed of the DFT MO calculations we used H–DAB and SnH$_3$ instead of *i*Pr–DAB and SnPh$_3$, respectively. Standard N–H and Sn–H bond distances were used [61].

Acknowledgements: The Netherlands Foundation for Chemical Research (SON), the Netherlands Organisation for Scientific Research (NWO), the University of Nottingham, together with COST D4 Action and the European Scientific Network "Organometallic Photochemistry", are thanked for financial support.

Received: June 17, 1996 [F394]

[1] H. A. Nieuwenhuis, D. J. Stufkens, A. Oskam, *Inorg. Chem.* **1994**, *33*, 3212.
[2] H. A. Nieuwenhuis, D. J. Stufkens, A. Vlček, Jr., *Inorg. Chem.* **1995**, *34*, 3879.
[3] H. A. Nieuwenhuis, A. van Loon, M. A. Moraal, D. J. Stufkens, A. Oskam, K. Goubitz, *Inorg. Chim. Acta* **1995**, *232*, 19.
[4] H. A. Nieuwenhuis, A. van Loon, M. A. Moraal, D. J. Stufkens, A. Oskam, K. Goubitz, *J. Organomet. Chem.* **1995**, *492*, 165.
[5] H. A. Nieuwenhuis, D. J. Stufkens, R. McNicholl, A. H. Al-Obaidi, C. G. Coates, S. E. J. Bell, J. J. McGarvey, J. Westwell, M. W. George, J. J. Turner, *J. Am. Chem. Soc.* **1995**, *117*, 5579.
[6] H. A. Nieuwenhuis, M. C. E. van de Ven, D. J. Stufkens, A. Oskam, K. Goubitz, *Organometallics* **1995**, *14*, 780.
[7] T. A. Oriskovich, P. S. White, H. H. Thorp, *Inorg. Chem.* **1995**, *34*, 1629.
[8] T. G. Kotch, A. J. Lees, S. J. Fuerniss, K. I. Papathomas, R. W. Snyder, *Inorg. Chem.* **1993**, *32*, 2570.
[9] T. G. Kotsch, A. J. Lees, *Chem. Mater.* **1991**, *3*, 25.
[10] N. B. Thornton, K. S. Schanze, *Inorg. Chem.* **1993**, *32*, 4994.
[11] O. Ishitani, M. W. George, T. Ibusuki, F. P. A. Johnson, K. Koike, K. Nozaki, S. Pac, J. J. Turner, J. R. Westwell, *Inorg. Chem.* **1994**, *33*, 4712.
[12] J. Hawecker, J. M. Lehn, R. Ziessel, *J. Chem. Soc. Chem. Commun.* **1983**, 536.
[13] J. Hawecker, J. M. Lehn, R. Ziessel, *Helv. Chim. Acta.* **1986**, *69*, 1990.
[14] G. Calzaferri, K. Hadener, J. Li, *J. Photochem. Photobiol. A. Chem.* **1992**, *64*, 259.
[15] C. Kutal, J. Corbin, G. Ferraudi, *Organometallics* **1987**, *6*, 553.
[16] M. Grätzel, *Energy Resources through Photochemistry and Catalysis*, Academic Press, New York, **1983**.
[17] M. Grätzel, *Coord. Chem. Rev.* **1991**, *111*, 167.
[18] D. J. Stufkens, *Comments Inorg. Chem.* **1992**, *13*, 359.
[19] K. S. Schanze, D. B. MacQueen, T. A. Perkins, L. A. Cabana, *Coord. Chem. Rev.* **1993**, *122*, 63.
[20] A. J. Lees, *Chem. Rev.* **1987**, *87*, 711.
[21] M. Wrighton, D. L. Morse, *J. Am. Chem. Soc* **1978**, *100*, 5790.
[22] J. C. Luong, R. A. Faltynek, M. S. Wrighton, *J. Am. Chem. Soc.* **1979**, *101*, 1597.
[23] K. Kalyanasundaram, *Proc. Indian Acad. Sci.* **1992**, *104*, 701.
[24] J. V. Caspar, T. J. Meyer, *J. Am. Chem. Soc.* **1983**, *105*, 5583.
[25] L. A. Worl, R. Duesing, P. Chen, L. Della Ciana, T. J. Meyer, *J. Chem. Soc. Dalton Trans.* **1991**, 849.
[26] M. W. George, F. P. A. Johnson, J. R. Westwell, P. M. Hodges, J. J. Turner, *J. Chem. Soc. Dalton Trans.* **1993**, 2977.
[27] B. D. Rossenaar, M. W. George, F. P. A. Johnson, D. J. Stufkens, J. J. Turner, A. Vlček, Jr., *J. Am. Chem. Soc.* **1995**, *117*, 11582.
[28] B. D. Rossenaar, D. J. Stufkens, A. Vlček, Jr., *Inorg. Chem.* **1996**, *35*, 2902.
[29] M. P. Aarnts, D. J. Stufkens, A. Oskam, J. Fraanje, K. Goubitz, *Inorg. Chim. Acta.*, in press.
[30] M. P. Aarnts, K. Peelen, F. Hartl, D. J. Stufkens, unpublished results.
[31] M. P. Aarnts, F. Hartl, K. Peelen, D. J. Stufkens, J. Fraanje, K. Goubitz, M. Wilms, E. J. Baerends, A. Vlček, Jr., *Inorg. Chem.* **1996**, *35*, 5468.
[32] M. W. Kokkes, T. L. Snoeck, D. J. Stufkens, A. Oskam, M. Christophersen, C. H. Stam, *J. Mol. Struct.* **1985**, *131*, 11.
[33] D. J. Stufkens, *Coord. Chem. Rev.* **1990**, *104*, 39.
[34] R. R. Andréa, W. G. J. de Lange, D. J. Stufkens, A. Oskam, *Inorg. Chim. Acta* **1988**, *149*, 77.
[35] M. P. Aarnts, M. P. Wilms, D. J. Stufkens, E. J. Baerends, A. Vlček, Jr., submitted for publication in *Organometallics*.
[36] M. P. Aarnts, D. J. Stufkens, A. Oskam, J. Fraanje, K. Goubitz, N. Veldman, A. L. Spek, *J. Organomet. Chem.*, in press.
[37] M. P. Wilms, D. J. Stufkens, E. J. Baerends, unpublished results.
[38] J. J. Turner, M. W. George, F. P. Johnson, J. R. Westwell, *Coord. Chem. Rev.* **1993**, *125*, 101.
[39] R. S. Lumpkin, E. M. Kober, L. A. Worl, Z. Murtaza, T. J. Meyer, *J. Phys. Chem* **1990**, *94*, 239.
[40] J. C. Luong, R. A. Faltynek, M. S. Wrighton, *J. Am. Chem. Soc.* **1980**, *102*, 7892.
[41] B. D. Rossenaar, E. Lindsay, D. J. Stufkens, A. Vlček, Jr., *Inorg. Chim. Acta.* **1996**, *250*, in press.
[42] B. D. Rossenaar, C. J. Kleverlaan, M. C. E. van de Ven, D. J. Stufkens, A. Vlček, Jr., *Chem. Eur. J.* **1996**, *2*, 228.
[43] P. I. Djurovich, R. J. Watts, *Inorg. Chem.* **1993**, *32*, 4681.
[44] M. P. Aarnts, D. J. Stufkens, A. Vlček, Jr., submitted for publication in *Inorg. Chim. Acta.*
[45] *Grams/386* implemented in WIN-IR software, Galactic Industries Corporation and Digilab Division, Bio-Rad Laboratories, **1991–1993**.
[46] C. A. Parker, W. T. Rees, *Analyst (London)* **1960**, *85*, 587.
[47] M. W. George, M. Poliakoff, J. J. Turner, *Analyst* **1994**, *119*, 551.
[48] M. W. George, Ph.D. Thesis, University of Nottingham, **1990**.
[49] E. J. Baerends, D. E. Ellis, P. Ros, *Chem. Phys* **1973**, *2*, 52.
[50] E. J. Baerends, P. Ros, *Int. J. Quantum Chem.* **1978**, *S12*, 169.
[51] P. M. Boerrigter, G. te Velde, E. J. Baerends, *Int. J. Quantum Chem.* **1988**, *33*, 87.
[52] G. te Velde, E. J. Baerends, *J. Comput. Phys.* **1992**, *99*, 84.
[53] R. G. Parr, W. Yang, *Density Functional Theory of Atoms and Molecules*, Oxford University Press, New York, **1989**.
[54] S. H. Vosko, L. Wilk, M. J. Nusair, *Can. J. Phys.* **1980**, *58*, 1200.
[55] A. D. Becke, *J. Chem. Phys.* **1986**, *84*, 4524.
[56] A. D. Becke, *Phys. Rev.* **1988**, *A38*, 3098.
[57] J. P. Perdew, *Phys. Rev.* **1986**, *B33*, 8822.
[58] J. P. Perdew, *Phys. Rev.* **1986**, *B34*, 7406.
[59] E. J. Baerends, O. V. Gritsenko, R. van Leeuwen in *Chemical Applications of Density Functional Theory* (Eds.: B. B. Laird, R. Ross, T. Ziegler), *ACS Symp. Ser.* **1996**, *629*, 20.
[60] M. P. Wilms, Free University Amsterdam, Internal Report **1995**.
[61] J. E. Huheey, *Inorganic Chemistry, Principles of Structure and Reactivity*, 3rd ed., New York, **1983**.
[62] M. J. A. Kraakman, B. de Klerk-Engels, P. P. M. de Lange, K. Vrieze, W. J. J. Smeets, A. L. Spek, *Organometallics* **1992**, *11*, 3774.
[63] F. A. Cotton, C. S. Kraihanzel, *J. Am. Chem. Soc.* **1962**, *84*, 4432.

  0947-6539/96/0212-1565 $ 15.00+.25/0